ARPA-NRL INFRARED INTEGRATED OPTICS PROGRAM. ANNUAL TECHNICAL REPORT TO ADVANCED RESEARCH PROJECTS AGENCY

T. G. Giallorenzi, et al

Naval Research Laboratory

Prepared for:

Advanced Research Projects Agency

April 1974

UNCLASSIFIED

SECURITY CLASSIFICATION OF THIS PAGE *(When Data Entered)*

REPORT DOCUMENTATION PAGE		READ INSTRUCTIONS BEFORE COMPLETING FORM
1. REPORT NUMBER NRL Memorandum Report 2783	2. GOVT ACCESSION NO.	3. RECIPIENT'S CATALOG NUMBER AD-780 780
4. TITLE *(and Subtitle)* ARPA-NRL INFRARED INTEGRATED OPTICS PROGRAM - ANNUAL TECHNICAL REPORT TO ADVANCED RESEARCH PROJECTS AGENCY		5. TYPE OF REPORT & PERIOD COVERED Annual Report 6. PERFORMING ORG. REPORT NUMBER
7. AUTHOR(s) T. G. Giallorenzi and John Warner		8. CONTRACT OR GRANT NUMBER(s)
9. PERFORMING ORGANIZATION NAME AND ADDRESS Naval Research Laboratory Washington, D.C. 20375		10. PROGRAM ELEMENT, PROJECT, TASK AREA & WORK UNIT NUMBERS NRL Prob. 65N01-38 ARPA Order No. 2327
11. CONTROLLING OFFICE NAME AND ADDRESS Advanced Research Projects Agency		12. REPORT DATE April 1974 13. NUMBER OF PAGES 44
14. MONITORING AGENCY NAME & ADDRESS*(if different from Controlling Office)*		15. SECURITY CLASS. *(of this report)* UNCLASSIFIED 15a. DECLASSIFICATION/DOWNGRADING SCHEDULE

16. DISTRIBUTION STATEMENT *(of this Report)*

Approved for public release; distribution unlimited.

17. DISTRIBUTION STATEMENT *(of the abstract entered in Block 20, if different from Report)*

18. SUPPLEMENTARY NOTES

19. KEY WORDS *(Continue on reverse side if necessary and identify by block number)*

N/A

20. ABSTRACT *(Continue on reverse side if necessary and identify by block number)*

The ARPA-NRL integrated optics program is concerned with the development of an infrared integrated optical technology. This report discusses the NRL in-house program on thin film magneto-optical isolators. Both theoretical and experimental aspects have been studied in detail.

DD FORM 1 JAN 73 1473 EDITION OF 1 NOV 65 IS OBSOLETE S/N 0102-014-6601 | 1

UNCLASSIFIED

SECURITY CLASSIFICATION OF THIS PAGE *(When Data Entered)*

TABLE OF CONTENTS

List of Publications Made During This Reporting Period

1. J. Warner, "Faraday Optical Isolator/Gyrator Design in Planar Dielectric Waveguide Form", IEEE J-MTT 21 (12) 769 (Dec. 1973).

2. W.K. Burns and J. Warner, "Mode Conversion in Uniaxial Waveguides", JOSA (March 1974).

3. J. Warner, "Excitation of Hybrid Modes in Magneto-optic Waveguides", Applied Optics (June 1974).

4. J. Warner, "The Refractive Indices of Some Garnet Crystals at 1.15 μm", Materials Research Bulletin (April 1974).

5. J. Warner, "Non-Reciprocal Magneto-optic Waveguides", Paper MB11 - New Orleans Conference OSA Pub. No. 74CH0870-6QEC (1974).

6. J. Warner, "Non-Reciprocal Magneto-optic Waveguides", submitted to IEEE JMTT (Jan. 75 special issue on integrated optics).

ANNUAL TECHNICAL REPORT

Reporting Period
1 December 1972 - 31 January 1974

1.	ARPA Order	2327
2.	Program Code Number	3D10
3.	Name of Contractor	Naval Research Laboratory Optical Sciences Division
4.	Effective Date of Contract	1 December 1972
5.	Contract Expiration Date	Continuing
6.	Amount of Contract	$90 K
7.	Contract Number	N/A
8.	Principal Investigator	Dr. T. G. Giallorenzi
9.	Phone Number	(202) 767-3209
10.	Scientific Officer	Dr. C. M. Stickley
11.	Title of Work	A Coordinated Research Program to Develop Infrared Integrated Optics

Sponsored by

ADVANCED RESEARCH PROJECTS AGENCY
ARPA Order No. 2327

1. INTRODUCTION

The main aim of this study is to design and demonstrate a planar optical waveguide version of an optical isolator employing the Faraday effect. This effect produces a rotation of the plane of polarization of linearly polarized light as it passes through a bulk magneto-optic medium. The rotation is right-handed (say) for light travelling with the magnetic field and left-handed (say) for light against the field. This non-reciprocal nature has been exploited at microwave (waveguide modes) and optical (bulk-wave modes) frequencies to make one-way transmission devices or isolators[1]. The situation is complicated in planar optical waveguides because circularly polarized propagation modes (which are used to explain the optical rotation of linearly polarized light) do not normally propagate in planar waveguides.

In this annual technical report we first of all summarize the essential features of a bulk-wave optical isolator, indicating what refinements over the basic configuration are required before a dielectric waveguide analog can be conceived. We then outline our path towards a practical design of dielectric waveguide isolator. This particular design has been given a thorough theoretical analysis, as outlined in section 3, and a practical version based on magnetic garnet films has been the subject of our experimental program. We give design data in section 4 and at the end of the report give a summary of our achievements to date. Certain experimental aspects of the program, such as the technique for determining waveguide thickness and refractive index parameters, should find application outside the scope of this immediate study, and these techniques are described in section 5 of the report.

2. BASIC DESIGN CONSIDERATIONS

2.1. Bulk-wave Optical Isolators

Figure 1 illustrates the longitudinal magneto-optic, or Faraday effect which is exploited in the design of optical isolators and circulators. An optical beam is sent through a magneto-optic crystal parallel to an applied magnetic field. Linearly polarized light travelling with the field will find its polarization direction rotated as a right hand screw whereas light travelling against the field is rotated in the opposite sense (a left hand screw in our example). This rotation is similar to that experienced in optically active crystals with one important difference; the magnetic medium experiences right- and left-hand rotation whereas the handedness of rotation in an optically active medium is not changed by reversing

Manuscript submitted April 2, 1974.

the propagation direction. If the path length in the magneto-optic crystal is such that a 45° rotation is achieved we are able by the simple addition of two linear polarizers at suitable azimuth orientations, to devise "one-way" transmission characteristics which constitute an optical isolator. Figure 2 shows that the polarizers are set at 45° to each other. Vertically polarized light travelling with the applied magnetic field passes through the input polarizer, is then rotated with a right-hand screw motion to 45° azimuth where it is correctly oriented to pass through the second polarizer. If this 45° polarized light is sent back against the field direction it would be rotated with a left-hand screw motion to a 90° azimuth to be blocked by the polarizer at 0° azimuth. In this way a combination of two polarizers set at 45° to each other and a 45° Faraday rotator will act as an optical isolator, permitting transmission in one direction only.

Waveguide modes in planar dielectric waveguides have their electric vectors vibrating in orthogonal planes. The simple bulk isolator described above will <u>not</u> therefore carry over to a waveguide version because the input and output polarizations are at 45°, not 0 or 90°. A second active element must be included so that the output polarization is brought back to 0° azimuth as illustrated in Fig. 3. A 45° optically-active rotator with a left-hand sense of rotation is inserted between the magnetic rotator and the second polarizer. This brings light vibrating at 45° azimuth to the vertical <u>for both directions of propagation</u>. Thus we can see intuitively that we need <u>two</u> active media to make an optical waveguide isolator. It is also implicit in these bulk wave isolators that the vertical and horizontal polarizations travel in-phase and the observed rotation of the direction of vibration is a consequence of the coupling between these polarizations. This phase-matching requirement carries over to the optical waveguide cases where the TE and TM modes must travel in phase.

2.2 Planar Dielectric Waveguide Isolators

A waveguide version of Fig. 3 has been proposed by Wang et al[2] in which magneto-optic and optically active (or anisotropic) crystals are placed, in tandem, on top of a dielectric waveguide as shown in Fig. 4. The waveguide mode fields penetrate into these regions but decay exponentially as they do so. It is possible to replace the optically active crystal with an anisotropic one in optical waveguide cases because TM modes have a component of electric field along the propagation direction and an anisotropic crystal can be oriented to provide a coupling term between this field component and the electric field of a TE mode.

The magnetic-optic effect only provides a weak coupling between TE and TM fields and since in Fig. 4 there is only a small penetration

of the mode field into the top layers the amount of mode conversion attainable would be quite small. This in turn calls for a requirement of accurate phase-matching between the TE and TM modes over long distances (on the order of 10 to 20 mms). Mode degeneracy cannot be achieved in a dielectric waveguide mode with optically isotropic materials (see Section 3.2) and so the waveguide structure supporting the magneto-optic and anisotropic crystals would itself have to be made from anisotropic materials.

A much better basic design is achieved if the essential materials (i.e. the magneto-optic and anisotropic layers) are regrouped as shown in Fig. 5. In this configuration the magneto-optic film forms the high index guiding layer and consequently is situated where the waveguide modes are most strongly located. Also the anisotropic layer, which is placed as a superstrate over the magnetic film, performs the double roles of providing mode-conversion complimentary to that of the magnetic film, and allowing the possibility of degenerate mode propagation or phase-matching. Figure 5 illustrates that the bulk wave analogue of this preferred geometry is one in which the anisotropic and optically active 45° rotators are sliced up into small sections which are then interleaved.

It is the basic design of Fig. 5 which was adopted in this program as the best candidate for experimental study. A survey of technically proven materials reveals that the best choice for experimentation comprises a magnetic garnet film grown on gadolinium gallium garnet with $LiIO_3$ acting as the anisotropic superstrate. Detailed design data for this system, based on the theory outlined in the next section is presented in Section 4 of this report.

3. THEORETICAL ANALYSIS OF OPTICAL WAVEGUIDE ISOLATOR

In this section we outline our theoretical analysis of an optical waveguide isolator/gyrator formed by a magneto-optic film sandwiched between an isotropic and an anisotropic layer as shown in Fig. 5. The mode-conversion analysis follows the ray-optical approach of Kogelnik et al[3] which includes the Goos Haenchen effects. That analysis is followed by a brief summary of how the anisotropic crystal which provides mode-conversion complimentary to the magnetic-film also provides for degenerate mode propagation.

3.1 Derivation of Coupled Mode Equations

In Fig. 6 we depict the zig-zag ray path of a TE wave in the waveguide. Mode conversion due to the magnetic film will occur along the paths BC and DE and that due to the anisotropic layer will occur upon reflection at CD. In each case the mode-conversion may be

described in terms of a coupling matrix where the off-diagonal terms represent the mode conversion coefficients. In general we write

$$\begin{bmatrix} TE_{out} \\ TM_{out} \end{bmatrix} = \begin{bmatrix} R_{11} & R_{12} \\ R_{21} & R_{22} \end{bmatrix} \begin{bmatrix} TE_{in} \\ TM_{in} \end{bmatrix}. \tag{3.1}$$

There is no mode conversion at the substrate boundary because the substrate is optically isotropic. The mode coupling matrix for reflection at the substrate boundary therefore has zero off-diagonal terms and is given by

$$\begin{bmatrix} R_S \end{bmatrix} = \begin{bmatrix} e^{2i\phi_e} & 0 \\ 0 & e^{2i\phi_m} \end{bmatrix} \tag{3.2}$$

where ϕ_e and ϕ_m are the Goos-Haenchen phase shifts associated with total internal reflection.

The anisotropic top layer is oriented in such a way that the permittivity tensor has the element ϵ_{23} non-zero when expressed in the coordinate system shown in Fig. 6. The mode coupling matrix for this reflection is given by(2)

$$\begin{bmatrix} R_T \end{bmatrix} = \begin{bmatrix} r\, e^{2i\phi_{ee}} & s\, e^{2i\phi_{em}} \\ -s\, e^{2i\phi_{em}} & r\, e^{2i\phi_{nm}} \end{bmatrix} \tag{3.3}$$

r, s, and the ϕ's have been related to material parameters by Wang et al(2) and, for convenience, these relations are tabulated in Appendix 1.

The mode coupling matrix applicable to a single passage through the magneto-optic film (either B to C or D to E) is derived in Appendix 2 and is given by

$$\begin{bmatrix} R_F \end{bmatrix} = e^{i\Delta} \begin{bmatrix} \cos\Psi & -\sin\Psi \\ \sin\Psi & \cos\Psi \end{bmatrix} \tag{3.4}$$

where $\Delta = -\dfrac{k_o n_f W}{\cos\theta}$ and $\Psi = -\dfrac{k_o G W \tan\theta}{n_f}$.

In adopting the analytical approach of Kogelnik et al[3] we use the matrices given by Eqs. 3.2, 3.3 and 3.4 to write down the TE and TM fields at each end of a complete zig-zag cycle. These are then related by a Taylor's series expansion to the field derivatives and, after some algebra, a pair of coupled differential equations emerge as

$$\left.\begin{aligned} \frac{dA_E}{dz} + i\left(\beta - \beta_E\right) A_E &= i K A_M \\ \frac{dA_M}{dz} + i\left(\beta - \beta_M\right) A_M &= i K A_E \quad . \end{aligned}\right\} \qquad (3.5)$$

A_E and A_M are the normalized TE and TM field amplitudes, β_E and β_M are the propagation constants of the TE and TM modes, and K is a coupling coefficient between the modes given by

$$K = \frac{s\cos^2\Psi + r \sin 2\Psi \cos(\phi_{ee} - \phi_{mm})}{\sqrt{b_E b_M}} \quad . \qquad (3.6)$$

b_E and b_M are the round trip bounce lengths illustrated in Fig. 6.

Equation 3.6 shows us how non-reciprocal mode conversion effects arise. If the propagation direction is reversed with respect to the magnetization direction, G, and hence Ψ will change sign. If we take care to match the magnitude of the two terms in the numerator of Eq. 3.6 then non-reciprocal mode conversion will be achieved; K being non-zero in the forward direction (say) but zero in the reverse direction. The interaction length for complete mode conversion may be found from the solutions to Eq. 3.5. If all the light is in the TE wave at Z = 0 then[4]

$$A_M(Z) = \frac{A_E(0)\, \sin[KZ(1 + Q^2)^{\frac{1}{2}}]}{[1 + Q^2]^{\frac{1}{2}}} \qquad (3.7)$$

where the phase mismatch factor $Q = \dfrac{\beta_E - \beta_M}{2K}$.

The maximum converted light intensity falls from 100% for $Q = 0$ to 50% for $Q = 0.80$. Such a value of Q allows one to estimate a practical tolerance on the phase-matching between TE and TM modes. This point is considered further in Section 4.

We see from Eq. 3.7 that complete conversion will occur in a distance ℓ_{opt} for which $\ell_{opt}K = \pi/2$. For the material parameters given in Section 4 we find that $\ell_{opt} \sim 2$ mms.

3.2 Phase-Matching for Degenerate Modes.

It is evident from Eq. 3.7 that the TE and TM modes between which we have arranged non-reciprocal coupling must propagate degenerately in order for complete TE to TM (and vice versa) conversion to take place. The diagonal terms of the mode-conversion matrices given by Eq. 3.2, 3.3, and 3.4 can be used to obtain expressions for the TE and TM propagation constants β_E and β_M. In order for a proper waveguide mode to exist, the phase delay of a zig-zag wave traversing the path A-B-C-D-E in the film (Fig. 6 refers) must be the same as that of an evanescent wave travelling in the substrate from A to E. After some algebra this requirement reduces mathematically to the following equations.

$$W_{TE} = \frac{\lambda}{2\pi}\left\{\frac{m\pi + \tan^{-1}\sqrt{\frac{(n_g^2 - n_y^2)}{(n_F^2 - n_g^2)}} + \tan^{-1}\sqrt{\frac{(n_g^2 - n_s^2)}{(n_F^2 - n_g^2)}}}{(n_F^2 - n_g^2)}\right\} \quad (3.8)$$

$$W_{TM} = \frac{\lambda}{2\pi}\left\{\frac{m\pi + \tan^{-1}\sqrt{\left(\frac{n_F^2}{n_x n_z}\right)^2 \frac{(n_g^2 - n_x^2)}{(n_F^2 - n_g^2)}} + \tan^{-1}\sqrt{\left(\frac{n_F}{n_s}\right)^4 \frac{(n_g^2 - n_s^2)}{(n_F^2 - n_g^2)}}}{(n_F^2 - n_g^2)}\right\} \quad (3.9)$$

where n_g is the effective guide index β/k_o and n_x, n_y, n_z are the refractive indices of the anisotropic top-layer. Degenerate modes are achieved when $W_{TE} = W_{TM}$ for a special value of n_g. Let us examine how this might be achieved if the anisotropic crystal is a negative uniaxial crystal with its optic axis in the film plane, roughly perpendicular to the propagation direction. For this configuration $n_x = n_z = n_o$, the ordinary refractive index and $n_y = n_e$,

the extraordinary refractive index. Now $n_F > n_s$ for any waveguide and this gives a tendency for W_{TM} to be greater than W_{TE} for any value of n_g due to the factor $(n_f/n_s)^4$ in the second arctan term in Eq. 3.9. Since in a negative uniaxial crystal $n_e < n_o$ we may find a value of n_g, close to n_o for which $(n_F^2/n_o^2)^2 (n_g^2 - n_o^2) < (n_g^2 - n_e^2)$ by just the amount to counter the factor $(n_f/n_s)^4$ yielding the result $W_{TE} = W_{TM}$. This situation is illustrated diagrammatically in Fig. 7.

4. DESIGN DATA FOR $LiIO_3$ - YIG - GGG WAVEGUIDE STRUCTURE

In order to attempt an experimental demonstration of a waveguide isolator in a short time scale (i.e. this reporting period) we must select our materials from those whose growth technology has been well developed for other reasons. Magnetic garnet films, grown epitaxially on to gadolinium gallium garnet (GGG), have received a lot of attention as magnetic bubble-domain memory media. These films are immediately suitable as optical waveguides, the magnetic films having a higher refractive index than GGG. The only change required for our purpose is to move the magnetization axis from normal to the film-plane to in the film-plane. This is achieved by altering the film composition slightly to change the lattice parameter mismatch between film and substrate. The films supplied to us by Dr. R. Henry of Rockwell International (Anaheim) have the composition $(LaY)_3\ Ga_{.33}\ Fe_{4.67}\ O_{12}$ and are grown by liquid phase epitaxy on to <111> oriented GGG. The transmission spectrum of the magnetic garnets demands the use of a 1.06 μm or, for even smaller absorption, a 1.152 μm laser beam. We use a cw HeNe laser operating at 1.152 μm in our experiments. Having settled on materials for the film and substrate the anisotropic top layer has to be chosen. The constraints are that the refractive indices should lie within a range (which proves to be small) over which mode-degeneracy could be achieved. This phase-matching requirement also demands that the material shall be either a negative uniaxial crystal, or a biaxial crystal with a large optic angle. It would appear that lithium iodate $LiIO_3$ is about the only suitable material with a developed growth technology.

Final design data may be obtained from the theory outlined in section 3 once the refractive indices of the materials are known. We know from section 3.2 that the optic axis of $LiIO_3$ should be set roughly perpendicular to the propagation direction in order to most readily achieve degenerate modes.

We first assume that the optic axis is indeed at 90° to the propagation direction and use eqs. 3.8 and 3.9 to calculate the thickness for which the TE and TM modes are degenerate. In bulk YIG the Faraday effect produces about 280°/cm optical rotation at 1.152 μm[6]. This corresponds to $G = 3.4 \times 10^{-4}$ and we therefore have all the information needed to compute the magneto optic mode-coupling, Ψ, given

by eq. 3.4. We next use eq. 3.6 to find the anisotropic mode coupling term, S, that yields zero net mode-conversion. S in turn is related to the angle, α, that the optic axis makes with the propagation direction via the equations given in appendix 1. It turns out that $\alpha \simeq 88$ degrees for our case and furthermore the phase-matching is insensitive to α as shown in fig. 8. This fact gives us the experimentally convenient feature that α can be readily altered by suitably tilting the waveguide assembly, and doing this will "tune-in" the correct value of S without materially altering the mode-degeneracy condition.

The required design data is summarized in Table 1. In this table the refractive indices of the garnet film and substrate were measured in the laboratory (see sec. 5.1) and those for the $LiIO_3$ top-layer were taken from the literature[5]. All other data emerges from calculations based on the theory given in section 3. For example the tolerance figure on the design film thickness of 1.395 μm is computed from the allowable phase-mismatch introduced by letting the maximum converted light intensity fall from 100% to 50%. It should be noted that a maximum of 50% mode conversion would still allow a good demonstration of non-reciprocal propagation because, in the reverse direction, we can still arrange for there to be no mode coupling.

5. LABORATORY TECHNIQUES

Of the several lab techniques and practices that were used in the course of this study we select the following three items as being noteworthy. The first describes a novel prism coupler assembly which allows the convenient observation of optical waveguiding in small samples - we have used samples of less than 3 mms long in any dimension. The second item is concerned with how a knowledge of coupling angles to excite waveguide modes can lead to accurate film thickness and refractive index determinations. Lastly we report the results of an experiment in which the thickness of a garnet waveguide film was reduced, in a controlled way, to a specified value using a sputter-etch technique.

5.1. Prism Coupling to Small Pieces of Optical Waveguides

Rutile has a sufficiently large refractive index to couple to all propagating modes in any garnet film waveguide. Rutile prisms available to us were of the 45°/45°/90° type with a 1cm square aperture. Such prisms would normally be larger than the waveguide samples and we therefore designed a mounting device in which an input and an output prism formed a planar mounting platform for the waveguide films. Small plastic rods transmitted the necessary coupling pressure to the right-angle corners of the prisms. A photograph of the assembly and an exploded view is shown in fig. 9, and a sketch

of the metallic components is given in fig. 10. The planar mounting surface was obtained by glueing the prisms to their brass holders and then rubbing the latter on emery cloth until observation under a high power microscope indicated that both prism top-surfaces were in the same plane. The whole assembly depicted in fig. 9 was mounted on a goniometer structure whose rotation axis could be adjusted to coincide with the right angle corner of the input prism. In this way large changes in incidence angle could be made without the need to reposition the beam to the prism corner.

When coupling to waveguides that are formed on thin substrates confusion can arise in identifying coupled-out waveguide modes from light that gets into the substrate at the first prism and out again at the output prism. The substrate radiation is exited by the incident beam being scattered into a large angular spread by the finite size of the right-angle corner of the input prism. We mount a screen on top of the goniometer which therefore rotates with the prism/waveguide assembly as the incidence angle is varied. Waveguide modes impinge on this screen at fixed locations whereas spots of radiation from the substrate move as the incidence angle is adjusted. Spots of light originating from waveguide modes are therefore readily distinguishable. Since we use a 1.152 μm laser beam all our observations were made with the aid of an image converter tube with an S1 photocathode.

5.2 Optical Waveguide Technique to Determine Film Thickness and Index.

In order that we might accurately specify the waveguide film thickness we must have good data on refractive indices, etc. Fortunately the waveguides themselves offer a good technique for refractive index and film thickness determination. The procedure is to accurately measure angles at which waveguide modes are exited. Knowing the refractive indices and prism-angle of the coupling prism we can calculate the propagation constants of these modes and then fit this data to the mode dispersion equations (eqs. 3.8, 3.9) using a least squares algorithm. Our prism data, obtained using a spectrometer operating at .6328 and 1.152 μm is summarized in table 2. The angles of incidence, θ_i at which waveguide modes are exited are related to the mode propagation constant β by the equation

$$\beta/k_o = n_p \sin(\alpha + \arcsin(\sin\theta_i/n_p)) \qquad (5.1)$$

where n_p is the prism refractive index and α is the angle between the incident and waveguide faces of the prism.

We programmed a Hewlett Packard Model 20 calculator to perform the function fitting. The program operates on the principle of selecting the value of film refractive index that gives the smallest standard deviation of film thickness determinations from each measured value of β. Usually the substrate refractive index is entered as a given value although it is possible to also vary that parameter to find the best fit. Obviously we have to record coupling angles for at least as many parameters that we wish values for (i.e. n_f and W, or n_f, W and n_s).

During our work we found that measuring several modes (3 to 6) to about ± 5 arc minutes accuracy would yield data with a standard deviation of about ± .003 μm on thickness and ± .0004 on refractive indices. Data for typical experiment is given in table 3. The goniometer reading at normal incidence, taken when the incident laser beam was reflected back along its path, served to calibrate the goniometer. Given the apparatus we find that a new film can be accurately characterized in less than half an hour, most time being spent in accurately fixing the coupling angles. We feel therefore that the technique described above offers a fast and accurate method to determine refractive indices and thicknesses of a rather special type of dielectric thin film, namely a film of up to 10 μm thick grown or deposited on to a lower refractive index substrate.

5.3 Sputter Etching Experiment to Reduce Film Thickness.

The final design data for the waveguide isolator experiment calls for a film thickness of 1.395 ± .02 μm. This figure depends upon the refractive index of the film. One of our samples (#6/2A/8) came to us from Rockwell International at 1.85 μm. We decided to remove material from this film by sputter etching. Our equipment was a VEECO Model 716 evaporating plant modified for RF sputtering at 13.56 MHz. The sputtering atmosphere was Argon gas at about 33 μm pressure. The anode to cathode separation was 15 mms. We chose to run at 50 watts RF power for a standard 15 minute period. After each period the sample was annealed in air at 800°C for 30 minutes. (We found that the sample was reduced somewhat in the sputtering apparatus due to heating in a low pressure environment.)

We repeated the above procedure 5 times to reduce the sample thickness from 1.847 μm to 1.382 μm. The measured data is summarized in table 4. Notice that the refractive index remained unchanged throughout the program. Figure 11 shows the sample thickness as a function of etch time. We have no explanation for the change in etch rate halfway through the experiment. Every effort was made to keep each sputter etch run the same in terms of gas pressure, RF power, etc. Surface roughness did not deteriorate markedly during the etching program.

6. EXPERIMENTS ON "ONE-WAY" MODE CONVERSION

Our experimental program to study non-reciprocal effects in optical waveguides is centered on a GGG-YIG-$LiIO_3$ waveguide of appropriate dimensions and a pair of rutile right-angle prisms acting as input/output couplers as depicted in fig. 12. We apply a magnetic bias field parallel to the propagation direction, couple into the TE mode and look at the amount of TM light that emerges. Non-reciprocal effects will be evident if the amount of mode-conversion changes when the bias field is reduced. The $LiIO_3$ orientation could be altered to minimize the smaller amount of conversion.

We mounted our waveguide on the rig described in section 5.1. The whole assembly was made of non-ferrous materials and so we were able to apply bias fields of about 100 Gauss with a suitably located electromagnet. A photograph of the assembled apparatus is given in fig. 13. An index-matching liquid under the rutile prisms minimizes mismatch reflections between the prism/YIG/GGG and $LiIO_3$-YIG-GGG regions.

Unfortunately our experiments have not been successful in demonstrating non-reciprocal effects. We attribute this to our failure to get $LiIO_3$ and garnet film in close enough contact. We have seen small amounts of mode conversion[7], insensitive to bias field reversal, but the TE and TM modes are not degenerate, indicating that the anisotropy of the $LiIO_3$ is not playing its part.

We have studied the mode dispersion waves for a 4 layer waveguide where we have introduced a thin gap of thickness t between the $LiIO_3$ and the garnet film. In fig. 14 we plot TE and TM curves for several values of t. We see that the gap is a critical factor in the location of the degenerate mode point. What happens is that the waveguide mode field decays into the gap and consequently the $LiIO_3$ is quickly screened from the mode. It only takes a $t = 0.1$ μm to remove any prospects of mode degeneracy. A gap of less than 0.1 μm infers a good optical contact. We could not optically contact our samples; a better optical finish will have to be obtained.

Alternatively we could place a high-index liquid layer between the $LiIO_3$ and the garnet film. If the refractive index of this liquid were greater than the effective guide index of the waveguide modes of interest then we would get a sinusoidal field pattern in the liquid layer instead of an exponential decay and the $LiIO_3$ would continue to be effective. We have such a liquid to hand; it is a Cargille Laboratories index matching liquid from their EH series. Its refractive index for the sodium D line is 2.04, we measure $n = 1.973$ and $\alpha = 0.9\ cm^{-1}$ at 1.152 μm. Unfortunately the material contains arsenic tribromide which reacts with the $LiIO_3$ and so we cannot use it. We have explored

the location of the degenerate mode operation points as a function of the thickness of a liquid layer of index 1.973. We see that the possibilities for degenerate modes persist to quite thick films as shown in fig. 15. Furthermore the phase-matching condition is insensitive to the exact liquid layer thickness if it is the range 0.5 to 1.0 μm.

SUMMARY

During this reporting period (1 December 1972 to 31 January 1974) we have identified the requirements for a magneto-optic isolator in an optical dielectric waveguide. These are that the provision of a magneto-optic medium is necessary but not sufficient. We must also provide an anisotropic medium to give us the capability of achieving degenerate modes in the waveguide, and to provide a mode coupling coefficient complimentary to the magnetic one. A periodic structure like Tien's serpentine circuit[8] cannot be used to make up for a mode mismatch since any such structure destroys the unique symmetry of the longitudinal magneto-optic effect which produces non-reciprocal phenomena. We have carried out a detailed theoretical study of the problem and are confident that our design is the best choice based on currently available materials. We use a layered structure in which an iron garnet film is grown epitaxially on to GGG and a $LiIO_3$ cyrstal is optically contacted to the film to form a superstrate. We have been successful in getting all the materials to the required dimensions etc. and have demonstrated our ability to measure critical parameters like film thickness to adequate accuracy.

So far we have failed to demonstrate non-reciprocal effects. We are confident that this is due to our inability to optically contact the $LiIO_3$ to the garnet film. The available samples had somewhat relaxed tolerances on optical flatness etc. New samples, with better optical finish will become available and we look forward to better success in optically contacting these satisfactorily.

An alternative avenue for further research would be to explore the possibilities of non-isotropic magneto-optic materials in which the magnetic and anisotropic mode coupling would take place in the same film. At this writing we have not begun to analyze such systems in any detail. A possible material class would be the orthoferrites. Study would be required to determine whether the phase-matching possibilities could lead to experimentally attractive situations like that found in the system described in this report. We refer here to the happy situation illustrated in fig. 8 where orientation adjustments change the mode coupling coefficient by large amounts whereas the phase-matching is hardly affected. Preliminary investigations suggest that this type of behavior does not normally occur in waveguides with anisotropic films.

APPENDIX 1

MODE CONVERSION MATRIX FOR REFLECTION AT ANISOTROPIC DIELECTRIC BOUNDARY

Wang et al[2] have derived expressions relating the reflection and mode conversion that takes place between TE and TM waves upon total internal reflection at a boundary between an isotropic medium of high refractive index and an optically uniaxial medium whose optic axis lies in the boundary plane. For convenience their expressions are copied out below.

$$\begin{bmatrix} TE_{OUT} \\ TM_{OUT} \end{bmatrix} = \begin{bmatrix} r_{ee} & -r_{em} \\ r_{em} & r_{mm} \end{bmatrix} \begin{bmatrix} TE_{in} \\ TM_{in} \end{bmatrix} \tag{1.1}$$

where

$$r_{ee} = \frac{1}{F}\left(\frac{G_1 J_2^*}{L_1} - \frac{G_2 J_1^*}{L_2}\right) \tag{1.2a}$$

$$r_{em} = \frac{2(p_1 - p_2) n_f \cos\theta}{F K_{23}} \tag{1.2b}$$

$$r_{mm} = \frac{1}{F}\left(\frac{G_1^* J_2}{L_1} - \frac{G_2^* J_1}{L_2}\right) , \tag{1.2c}$$

and

$$F = \frac{G_1 J_2}{L_1} - \frac{G_2 J_1}{L_2} \tag{1.3a}$$

$$G_{1,2} = p_{1,2} K_{11} \cos\theta - i(n_g^2 - K_{11}) n_f \tag{1.3b}$$

$$J_{1,2} = n_f \cos\theta - i\, p_{1,2} \tag{1.3c}$$

$$L_{1,2} = n_g^2 K_{33} - K_{11} K_{33} - K_{11} p_{1,2}^2 . \tag{1.3d}$$

In the above expression p_1 and p_2 are the decay constants of the evanescent waves into the anisotropic layer, given by

$$p_{1,2}^2 = \frac{1}{2K_{11}} \left\{ A \pm \left[B^2 - 4\, K_{11} K_{23}^2 (n_g^2 - K_{11}) \right]^{\frac{1}{2}} \right\} \quad (1.4a)$$

where

$$A = n_g^2 (K_{11} + K_{33}) - K_{11}(K_{22} + K_{33}) \quad (1.4b)$$

$$B = n_g^2 (K_{11} - K_{33}) - K_{11}(K_{22} - K_{33}) \quad (1.4c)$$

$$C = n_g^2 (K_{11} + K_{33}) - K_{11}(K_{22} - K_{33}) \quad . \quad (1.4d)$$

n_g is the effective guide index β/K_o and the K_{ij} are the permittivity tensor coefficients for the uniaxial layer. If the optic axis makes an angle of α with the propagation direction we find that

$$(K_{ij}) \quad \begin{bmatrix} n_o^2 & 0 & 0 \\ 0 & n_o^2 \cos^2\alpha + n_e^2 \sin^2\alpha & (n_e^2 - n_o^2)\cos\alpha\sin\alpha \\ 0 & (n_e^2 - n_o^2)\cos\alpha\sin\alpha & n_o^2 \sin^2\alpha + n_e^2 \cos^2\alpha \end{bmatrix} . \quad (1.5)$$

r_{ee}, r_{em} and r_{mm} are, in general, complex quantities. In section 3 of this report they are referred to in a modules and phase angle form. Wang et al[2] also show that we may write

$$r_{ee} = r\, e^{i\phi_{ee}}$$

$$r_{mm} = r\, e^{i\phi_{mm}}$$

$$r_{em} = S\, e^{i\frac{1}{2}(\phi_{ee} + \phi_{mm})} \quad .$$

For a given configuration r, S, ϕ_{ee} and ϕ_{mm} are readily obtained by numerical computation from eqs. 1.2.

APPENDIX 2

MODE CONVERSION MATRIX FOR CUBIC MAGNETO-OPTIC WAVEGUIDING FILM

The amount of TE to TM mode conversion (and vice versa) that takes place during a single traverse of the "zig-zag" plane wave that makes up the waveguide mode may be described in terms of a matrix R where

$$\begin{bmatrix} TE_{OUT} \\ TM_{OUT} \end{bmatrix} = \begin{bmatrix} R \end{bmatrix} \begin{bmatrix} TE_{IN} \\ TM_{IN} \end{bmatrix} . \qquad (2.1)$$

In the following analysis we work out expressions for the coefficients of R in terms of the properties of the magneto-optic film, which we assume to be optically isotropic.

In general the dielectric properties of a magneto-optic medium may be described by a gyration vector $\underline{g}$ which features in the equation relating $\underline{D}$ and $\underline{E}$ as

$$\underline{D} = \underline{\underline{\epsilon}}\ \underline{E} + i\ \underline{E} \times \underline{g} \quad . \qquad (2.2)$$

For an isotropic medium the dependence of $\underline{g}$ on the external field is one of simple proportionality, $\underline{\underline{\epsilon}}$ too reduces to a scalar n^2, where n is the refractive index. We define a right-hand set of coordinate axes x_i (i=1,2,3) with x_3 parallel to the waveguide propagation direction, x_2 also in the film plane and x_1 directed normal to the film form substrate to top layer (fig. 6 refers). The dielectric constant tensor referred to these axes is therefore given by

$$D_i = \sum_{j=1}^{3} K_{ij}^{x} E_j = n^2 E_i + i \sum_{j=1}^{3} \sum_{k=1}^{3} e_{ijk} E_j g_K \qquad (2.3)$$

where e_{ijk} is an antisymmetrical unit tensor.

If we assume that the magnetization is directed along the propagation direction, x_3, then $g_1 = g_2 = 0$ and $g_3 = G$(say). The dielectric tensor then takes on the special form

$$\left(K^x_{ij}\right) = \begin{bmatrix} n^2 & iG & 0 \\ -iG & n^2 & 0 \\ 0 & 0 & n^2 \end{bmatrix}. \qquad (2.4)$$

It will be convenient to transform the problem to new axes (y_i) where y_3 is directed along the "zig-zag" ray path in the film. If y_2 is set parallel to x_2 then the TE and TM electric fields will be directed along y_2 and y_1 respectively. The transformation matrix relating (x_i) and (y_i) is given by $y_i^{\pm} = a_{ij}^{\pm} x_j$. The $\pm$ superscript refers to the "up" and "down" rays respectively. If θ is the angle of incidence of the "zig-zag" wave (fig. 6) then we write

$$\left(a_{ij}\right)^{\pm} = \begin{bmatrix} \cos(\pi/2 - \theta) & 0 & \mp \sin(\pi/2 - \theta) \\ 0 & 1 & 0 \\ \pm\sin(\pi/2-\theta) & 0 & \cos(\pi/2 - \theta) \end{bmatrix}. \qquad (2.5)$$

We can now refer the dielectric tensor of the magnetic film to the axes (y_i) and find that

$$\left(K^v_{ij}\right)^{\pm} = a^{\pm}_{ik}\, a^{\pm}_{j\ell} \left(K^x_{k\ell}\right) = \begin{bmatrix} n^2 & iG\sin\theta & 0 \\ -G\sin\theta & n^2 & \mp iG\cos\theta \\ 0 & \pm iG\cos\theta & n^2 \end{bmatrix}. \qquad (2.6)$$

If we assume an $e^{i(\omega t - \underline{k}\cdot\underline{r})}$ dependence of the fields the electromagnetic wave equations reduces to

$$k^2\,\underline{E} - \underline{k}(\underline{k}\cdot\underline{E}) = k_o^2\,\underline{K}^y\cdot\underline{E} \quad . \qquad (2.7)$$

Let us assume a solution of the form $e^{i(\omega t - \gamma k_o Z)}$ where, for ease of indexing we replace y_3 by Z_1, y_2 by y, and y_1 by x. We therefore obtain from eq. 2.7 that

$$\gamma^2(\underline{i}\,E_x + \underline{j}\,E_y) = \begin{bmatrix} n^2 & iG\sin\theta \\ -iG\sin\theta & n^2 \end{bmatrix} \begin{bmatrix} \underline{i}\,E_x \\ \underline{j}\,E_y \end{bmatrix} \qquad (2.8)$$

and hence $\gamma^2 = (n^2 \pm G\sin\theta)$ and $E_x = \pm iE_y$. (2.9)

Equation 2.9 shows us the well known result that the eigenmodes of propagation are circularly polarized with propagation constants

$$\gamma^{r,\ell} = (n^2 \pm G\sin\theta)^{\frac{1}{2}}. \qquad (2.10)$$

Notice that the <u>same</u> result is obtained for both the "up" and "down" rays. In order to work out the mode-conversion that takes place in one transit (up or down) of the zig-zag path we decompose each of the TE and TM polarizations into two counterrotating circularly polarized modes. We let these propagate along the ray path length $w/\cos\theta$ and then reform the TE and TM polarizations. Thus

$$E_x(z) = \frac{E_x(0)}{2} e^{-ik_o\gamma^r z} + \frac{E_x(0)}{2} e^{-ik_1\gamma^\ell z} + i\frac{E_y(0)}{2} e^{-ik_o\gamma^r z} - i\frac{E_y(0)}{2} e^{-ik_o\gamma^\ell z} \qquad (2.11)$$

$$E_y(z) = -i\frac{E_x(0)}{2} e^{-ik_o\gamma^r z} + i\frac{E_x(0)}{2} e^{-ik_o\gamma^\ell z} + \frac{E_y(0)}{2} e^{-ik_o\gamma^r z} + \frac{E_y(0)}{2} e^{-ik_o\gamma^\ell z} \qquad (2.12)$$

At z=0 we find that $E_x(z=0) = E_x(0)$ and $E_y(z=0) = E_y(0)$. Equations 10 and 11 can be factorized by noting, for example, that

$$-ik_o\gamma^r z = \frac{-i(\gamma^r-\gamma^\ell)k_o z}{2} - \frac{i(\gamma^r+\gamma^\ell)k_o z}{2}.$$

Thus

$$E_x(z) = e^{\frac{-ik_o(\gamma^r+\gamma^\ell)z}{2}} \left\{ E_x(0)\cos\left[\frac{k_o(\gamma^r-\gamma^\ell)z}{2}\right] + E_y(0)\sin\left[\frac{k_o(\gamma^r-\gamma^\ell)z}{2}\right] \right\} \qquad (2.13)$$

$$E_y(z) = e^{\frac{-ik_o(\gamma^r+\gamma^\ell)z}{2}} \left\{ -E_x(0) \sin\left[\frac{k_o(\gamma^r-\gamma^\ell)z}{2}\right] + E_y(0) \cos\left[\frac{k_o(\gamma^r-\gamma^\ell)z}{2}\right] \right\} . \quad (2.14)$$

From eq. 2.10 we find $\frac{\gamma^r+\gamma^\ell}{2} = n$ and $\frac{\gamma^r-\gamma^\ell}{2} = \frac{2G\sin\theta}{n}$ and, since we can identify TE modes with E_y and TM modes with E_x, we find that the matrix defined in eq. 2.1 can be written from eq. 2.13 and 2.14 as

$$\left[R^{UP}\right] = \left[R^{DOWN}\right] = e^{i\Delta} \begin{bmatrix} \cos\Psi & -\sin\Psi \\ \sin\Psi & \cos\Psi \end{bmatrix} \quad 2.15$$

where $\Delta = \frac{-k_o n W}{\cos\theta}$ and $\Psi = \frac{-k_o g W \tan\theta}{n}$. This is the desired matrix.

REFERENCES

1. J. Helszan, "Principles of Microwave Ferrite Engineering" Wiley-Interscience (1969).

2. S. Wang, M. Shah, J.D. Crow, "Studies of the Use of Gyrotropic and Anisotropic Materials for Mode-Conversion in Thin-Film Optical Waveguide Applications", J. Appl. Phys. 43 (4), 1861-1875 (April 1972).

3. H. Kogelnik, T.P. Sosnowski and H.P. Weber, "A Ray-Optical Analysis of Thin Film Polarization Converters", IEEE J. Quant. Elec. QE-9, (8) 795-800 (Aug. 1973).

4. S.E. Miller, "Coupled Wave Theory and Waveguide Applications", Bell Syst. Tech. Jour. 33, 661-719 (May 1954).

5. G. Nath, S. Haussuhl, "Large Nonlinear Optical Coefficient and Phase-Matched Second Harmonic Generation in $LiIO_3$, Applied Phys. Letters 14, 154-156 (1969).

6. Landölt-Bornstein, Physical Tables, New Series, Group III, Vol 4a, p. 344, Springer (Berlin) 1970.

7. J. Warner, "Excitation of Hybrid Modes in Magnetooptic Waveguides" Applied Optics 13.(5)(May 1974).

8. P.K. Tien, R.J. Martin, R. Wolfe, R.C. LeCrow, S.L. Blank, "Switching and Modulation of Light in Magnetooptic Waveguides of Garnet Films", Appl. Phys. Letters 21 (8), 394-396 (Oct. 1972).

TABLE 1

DESIGN DATA FOR $LiIO_3$-YIG-GGG WAVEGUIDE ISOLATOR FOR 1.152 μm OPERATION

Substrate

Single crystal $Gd_3\ Ga_5O_{12}$

Film grown epitaxially on to <111> surface

$n_s = 1.945 \pm .001$

Magneto-optic Film

$(LaY)_3\ Ga_{.33}\ Fe_{4.67}O_{12}$ grown by LPE

$n_f = 2.1783 \pm .0004$

$W = 1.395 \pm .02\ \mu m$

$G = 3.4 \times 10^{-4}$ ($\equiv$ 280°/cm Faraday rotation)

$\Psi = 2.43 \times 10^{-3}$ rad

m = 2 modes are degenerate, $\beta/k_o = 1.9568$, $\theta = 63.9°$

Top Layer

Single crystal $LiIO_3$ (optically contacted)

$n_o = 1.858$, $n_e = 1.716$

Optic axis about 88° from z in yz plane

Length for complete mode conversion $\simeq$ 2 mms

$\phi_{ee} - \phi_{mm} = 89.0° - 82.8° = 6.2°$

S = 0.0049

Waveguide decay constants into top layer

(a) for TE mode 1.08 μm

(b) for TM mode 1.70 μm.

TABLE 2

REFRACTIVE INDICES OF SYNTHETIC RUTILE AT 1.152 μm and .6328 μm

WAVELENGTH	n_o	n_e
.6328 μm	2.5833 ± .0003	2.8647 ± .0003
1.152 μm	2.4703 ± .0003	2.7254 ± .0003

Note: Measurements were made at 24°C.

TABLE 3

Typical data taken to determine film thickness and refractive index at 1.152 μ.

Prism angle - 45° 29'. Substrate refractive index - 1.945.

Sample No. 6/2A/7. Composition $(YLa)_3Ga_{.33}Fe_{4.67}O_{12}$.

Scale reading at normal incidence 75° 48'.

Scale Reading	Mode No.	θ	β/K
56°40'±1'	TE_o	19.13°	2.159
62°09'±2'	TE_1	13.65°	2.101
70°31'±5'	TE_2	5.28°	2.007
34°57'±1'	TM_o	40.85°	2.157
43°39'±2'	TM_1	32.15°	2.093
55°16'±5'	TM_2	20.53°	1.990

Least squares fitting yeilds thickness = 1.715 ± .008 μm
index = 2.1783 ± .0006

TABLE 4

Data from sputter etching experiment. Sample No. 6/2A/8, Composition $(YLa)_3Ga_{.33}Fe_{4.67}O_{12}$.

UNIT	ETCH TIME (MINS) TOTAL	PRISM COUPLING ANGLES ° TE_0	TE_1	TE_2	W (μm)	n
0	0	19.40	14.55	6.95	1.847	2.178
15	15	19.27	14.07	6.03	1.771	2.179
15	30	19.08	13.47	4.87	1.688	2.178
15	45	18.09	13.00	3.80	1.625	2.178
15	60	18.63	11.95	1.87	1.502	2.178
15	75	18.43	10.80	0.15	1.382	2.179

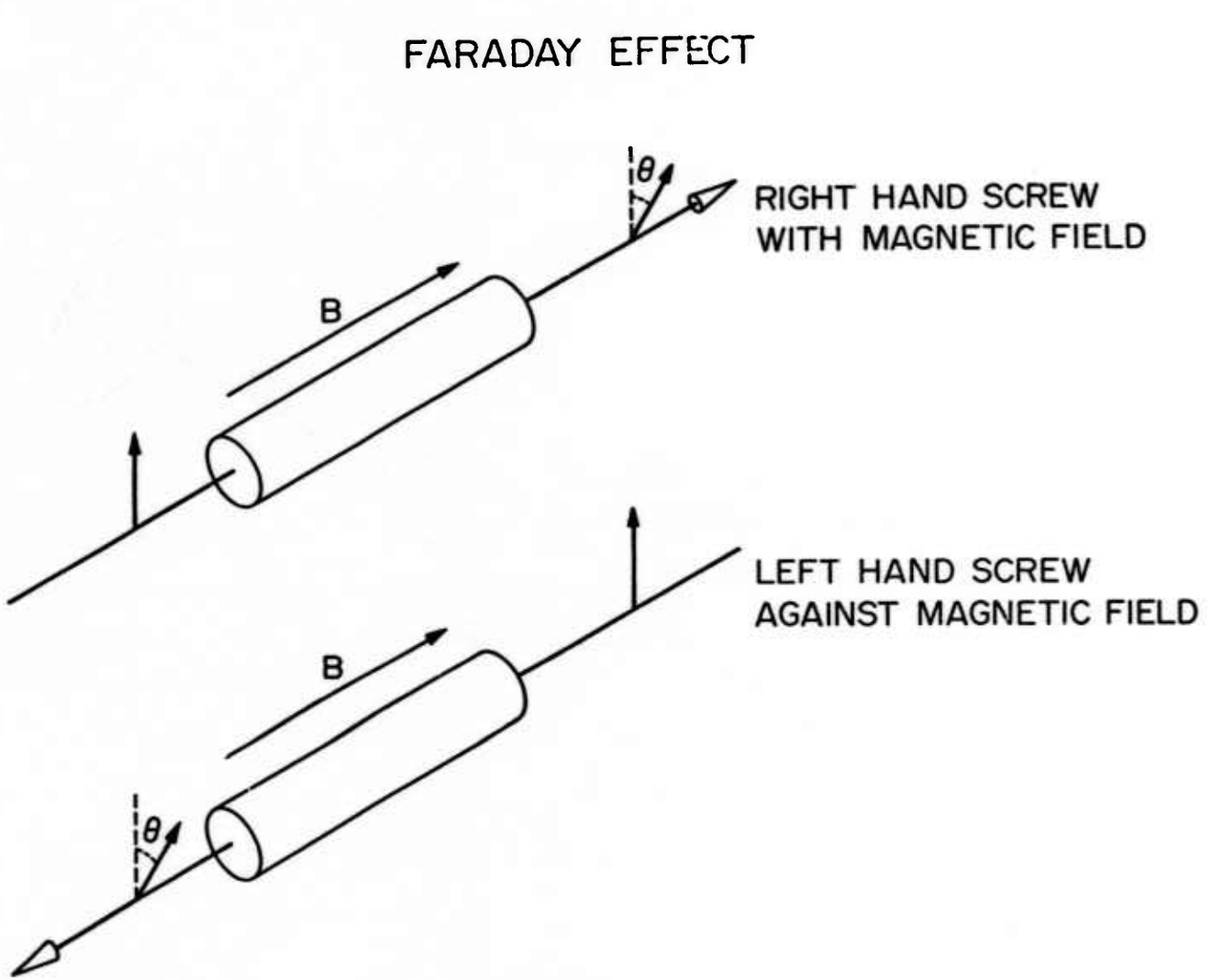
FARADAY EFFECT
θ
RIGHT HAND SCREW
WITH MAGNETIC FIELD
B
LEFT HAND SCREW
AGAINST MAGNETIC FIELD
B
θ

Figure 1

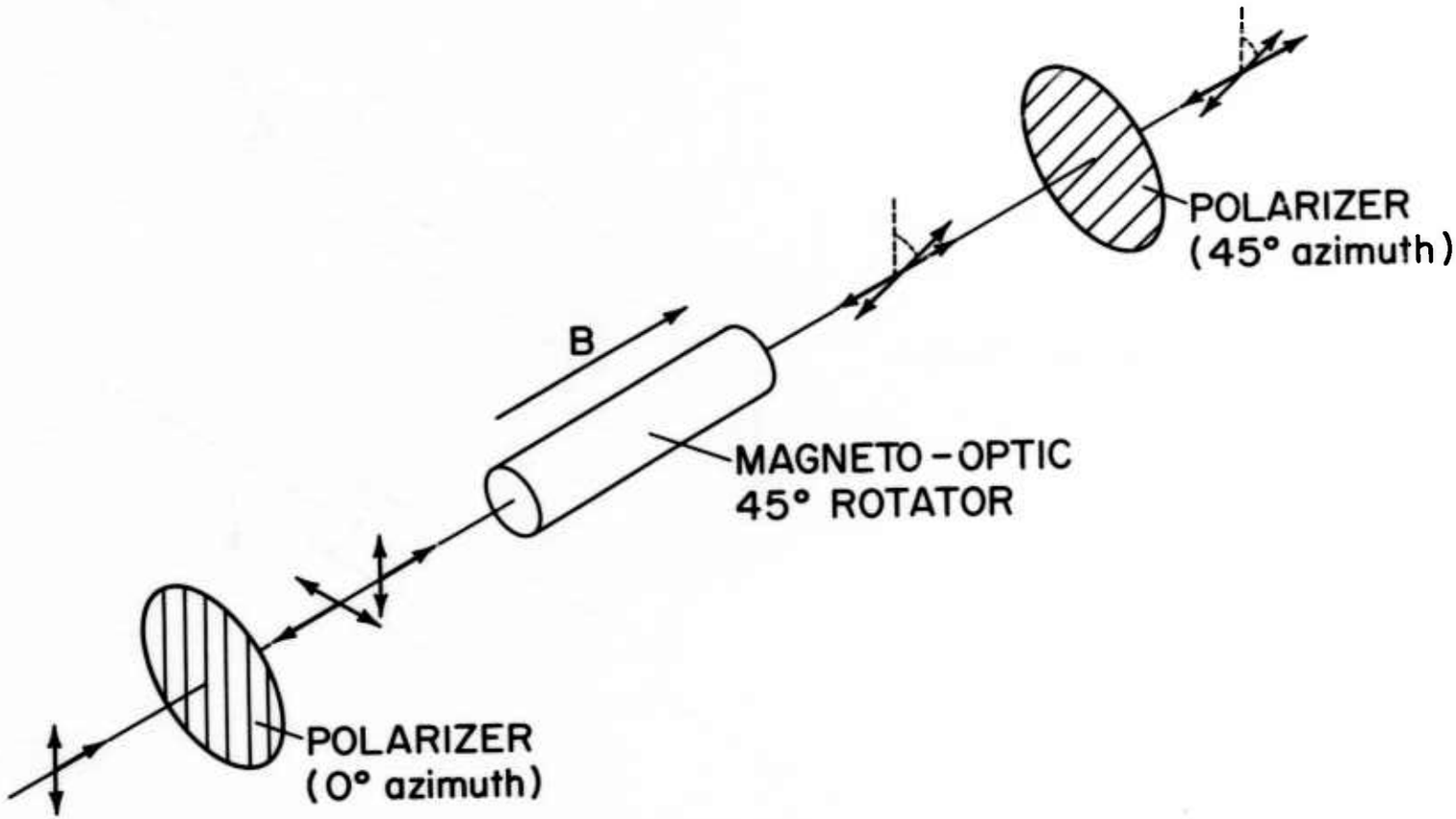
POLARIZER
(45° azimuth)
B
MAGNETO-OPTIC
45° ROTATOR
POLARIZER
(0° azimuth)

Figure 2

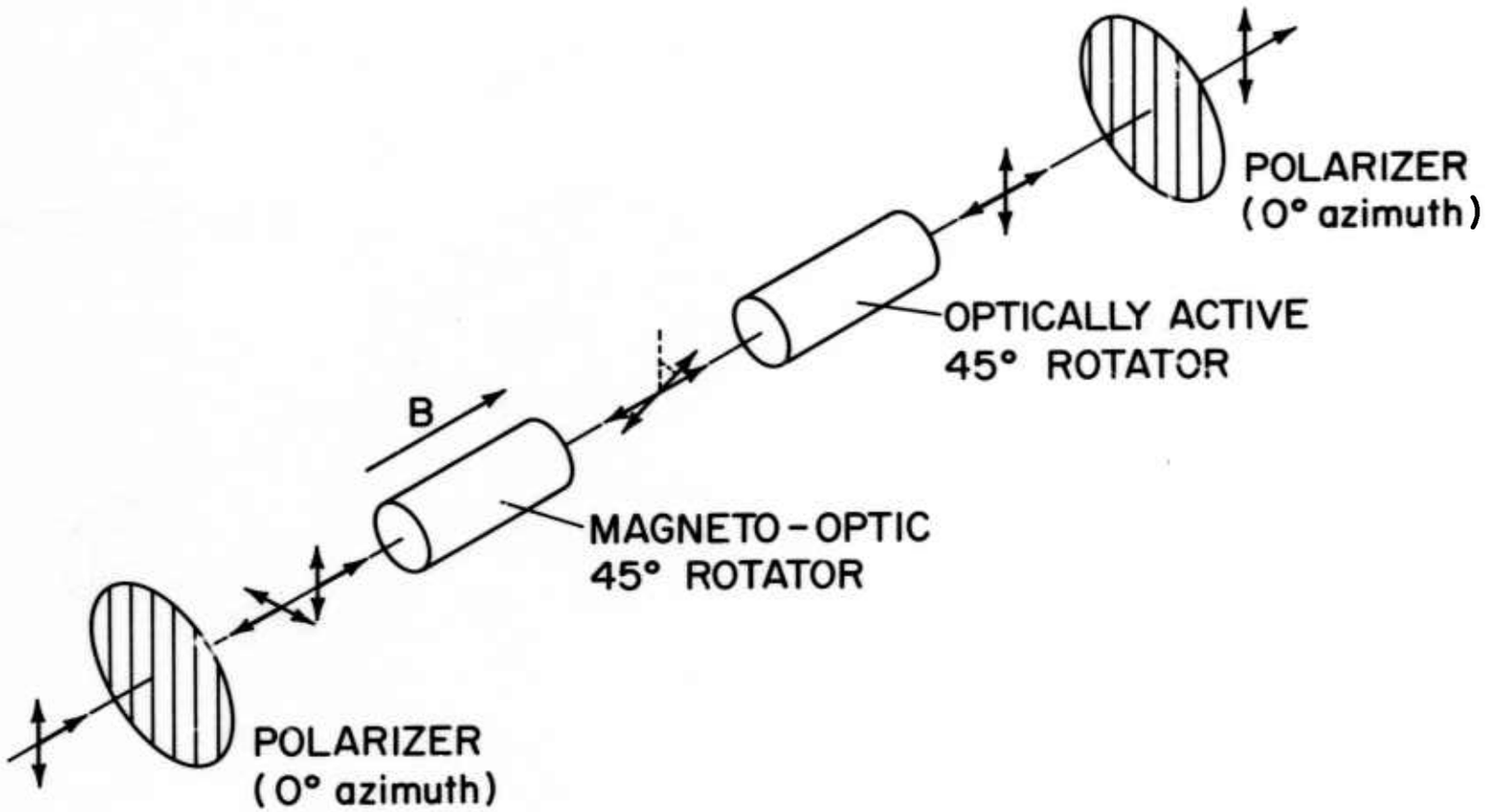
POLARIZER
(0° azimuth)
OPTICALLY ACTIVE
45° ROTATOR
B
MAGNETO-OPTIC
45° ROTATOR
POLARIZER
(0° azimuth)

Figure 3

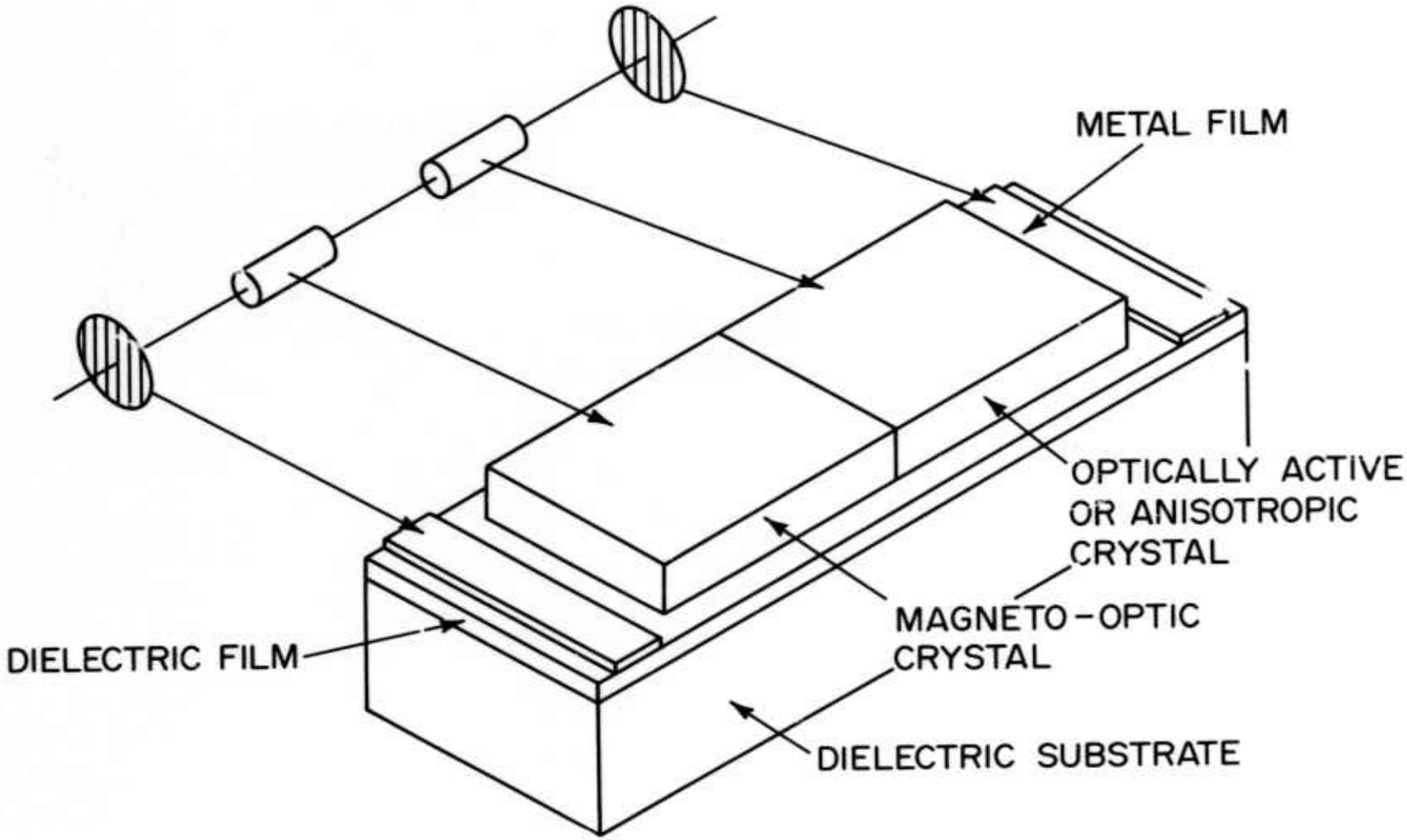
METAL FILM
OPTICALLY ACTIVE
OR ANISOTROPIC
CRYSTAL
MAGNETO-OPTIC
CRYSTAL
DIELECTRIC FILM
DIELECTRIC SUBSTRATE

Figure 4

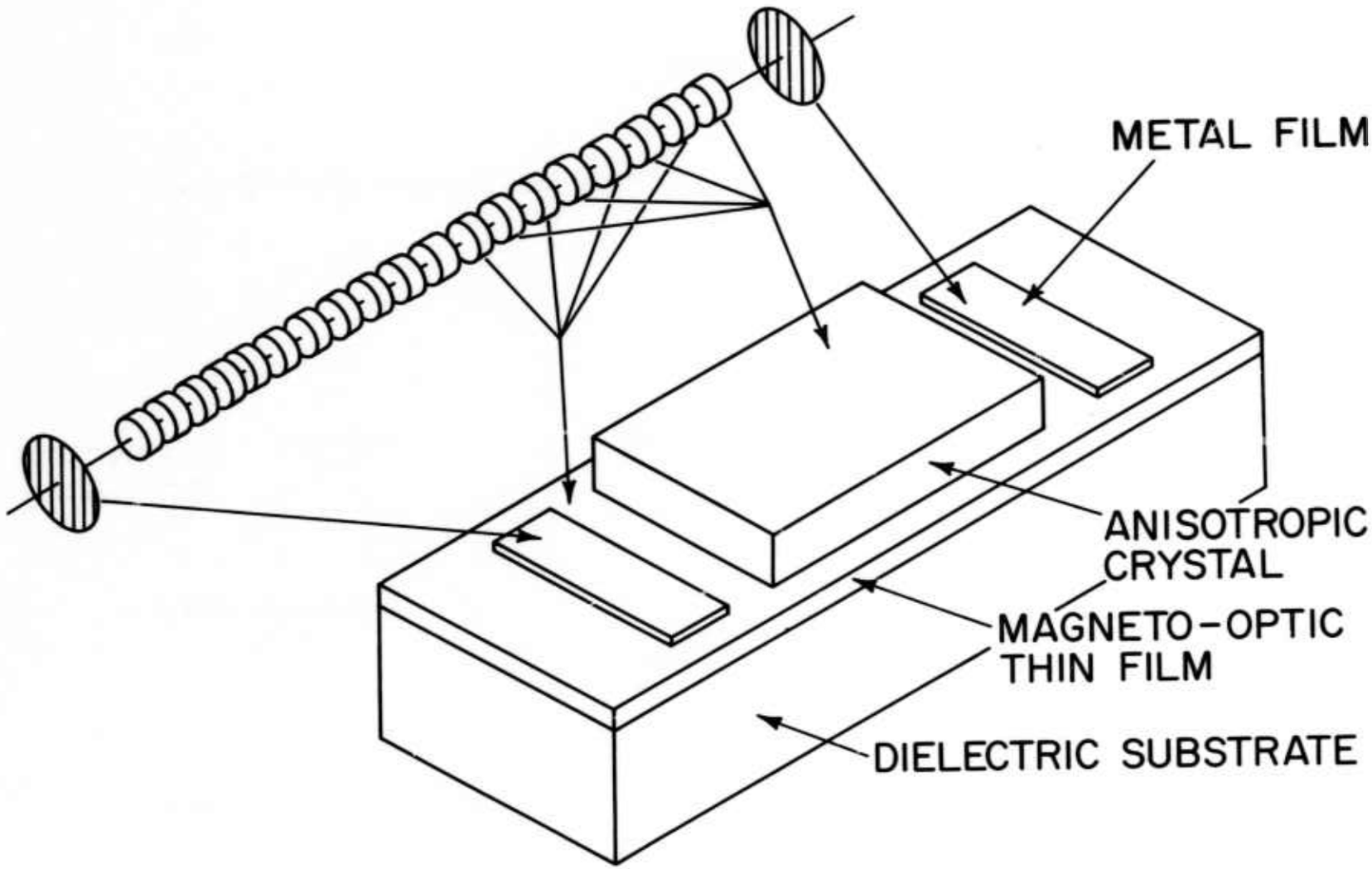
METAL FILM
ANISOTROPIC CRYSTAL
MAGNETO-OPTIC THIN FILM
DIELECTRIC SUBSTRATE

Figure 5

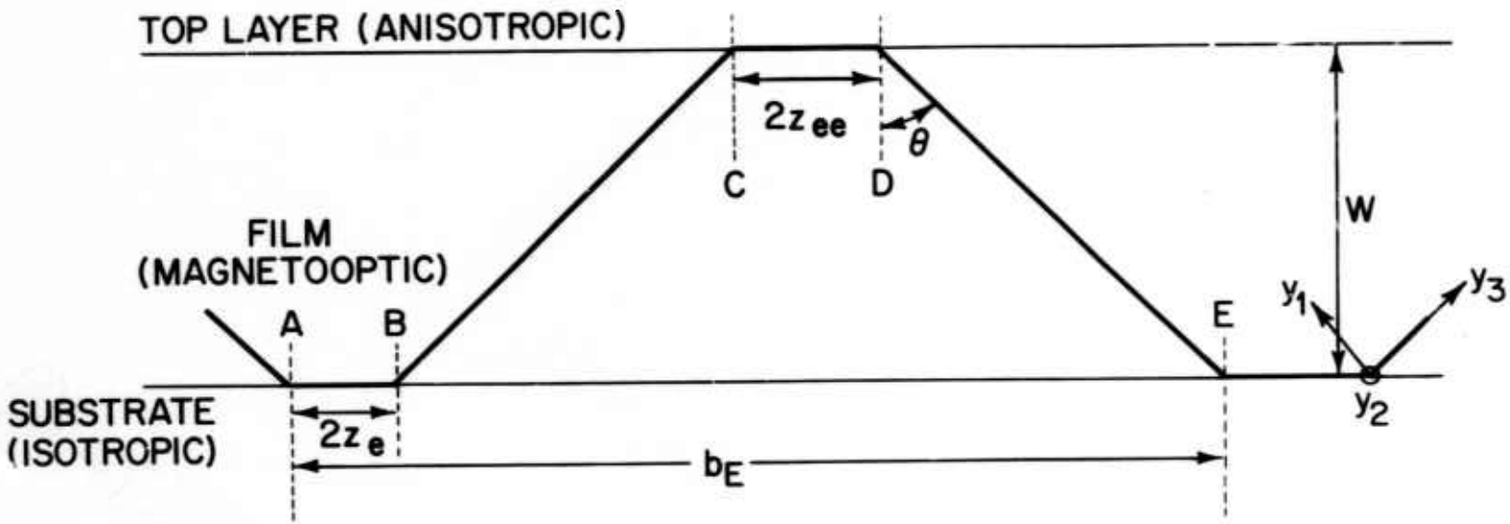

ZIG-ZAG RAY PATH OF TE-WAVE

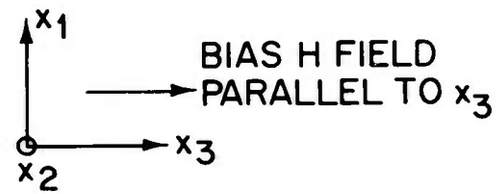

Figure 6

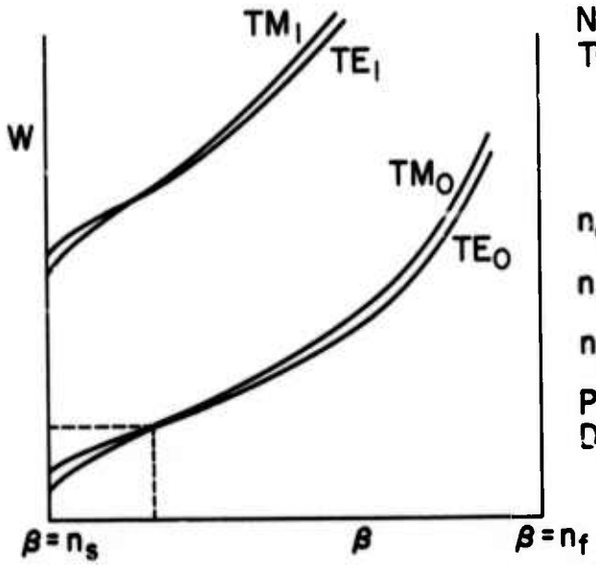

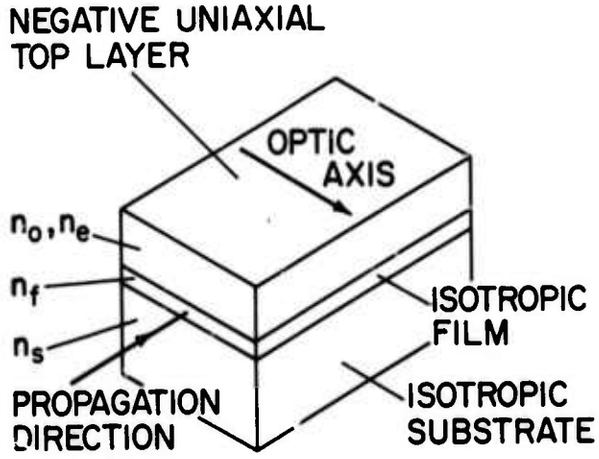

$$W_{TE} = \frac{\lambda}{2\pi}\left\{\frac{m\pi + \tan^{-1}\sqrt{\frac{(\beta^2 - n_e^2)}{(n_f^2 - \beta^2)}} + \tan^{-1}\sqrt{\frac{(\beta^2 - n_s^2)}{(n_f^2 - \beta^2)}}}{(n_f^2 - \beta^2)}\right\}$$

$$W_{TM} = \frac{\lambda}{2\pi}\left\{\frac{m\pi + \tan^{-1}\sqrt{\left(\frac{n_f}{n_o}\right)^4 \frac{(\beta^2 - n_o^2)}{(n_f^2 - \beta^2)}} + \tan^{-1}\sqrt{\left(\frac{n_f}{n_s}\right)^4 \frac{(\beta^2 - n_s^2)}{(n_f^2 - \beta^2)}}}{(n_f^2 - \beta^2)}\right\}$$

Figure 7

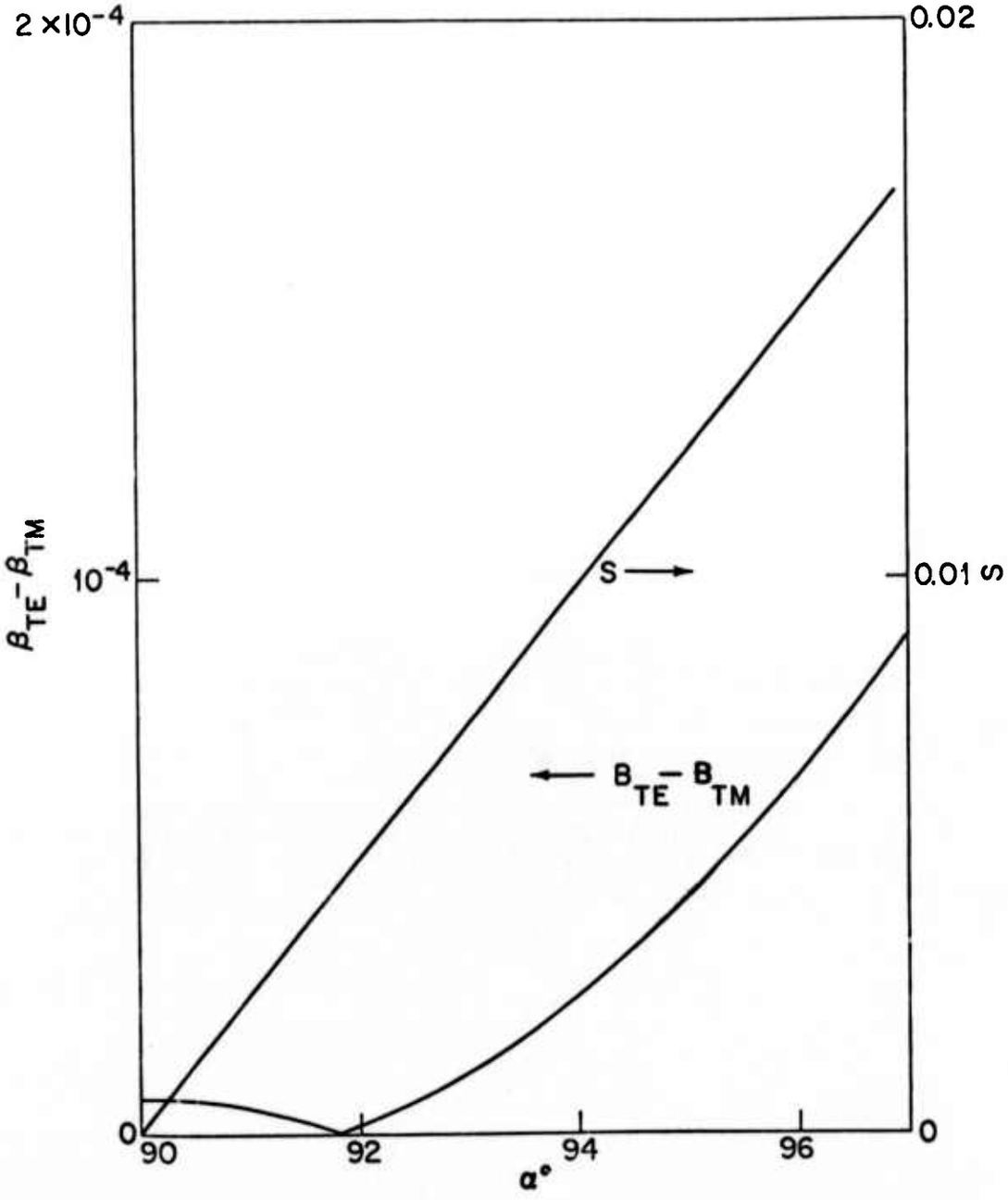

Figure 8

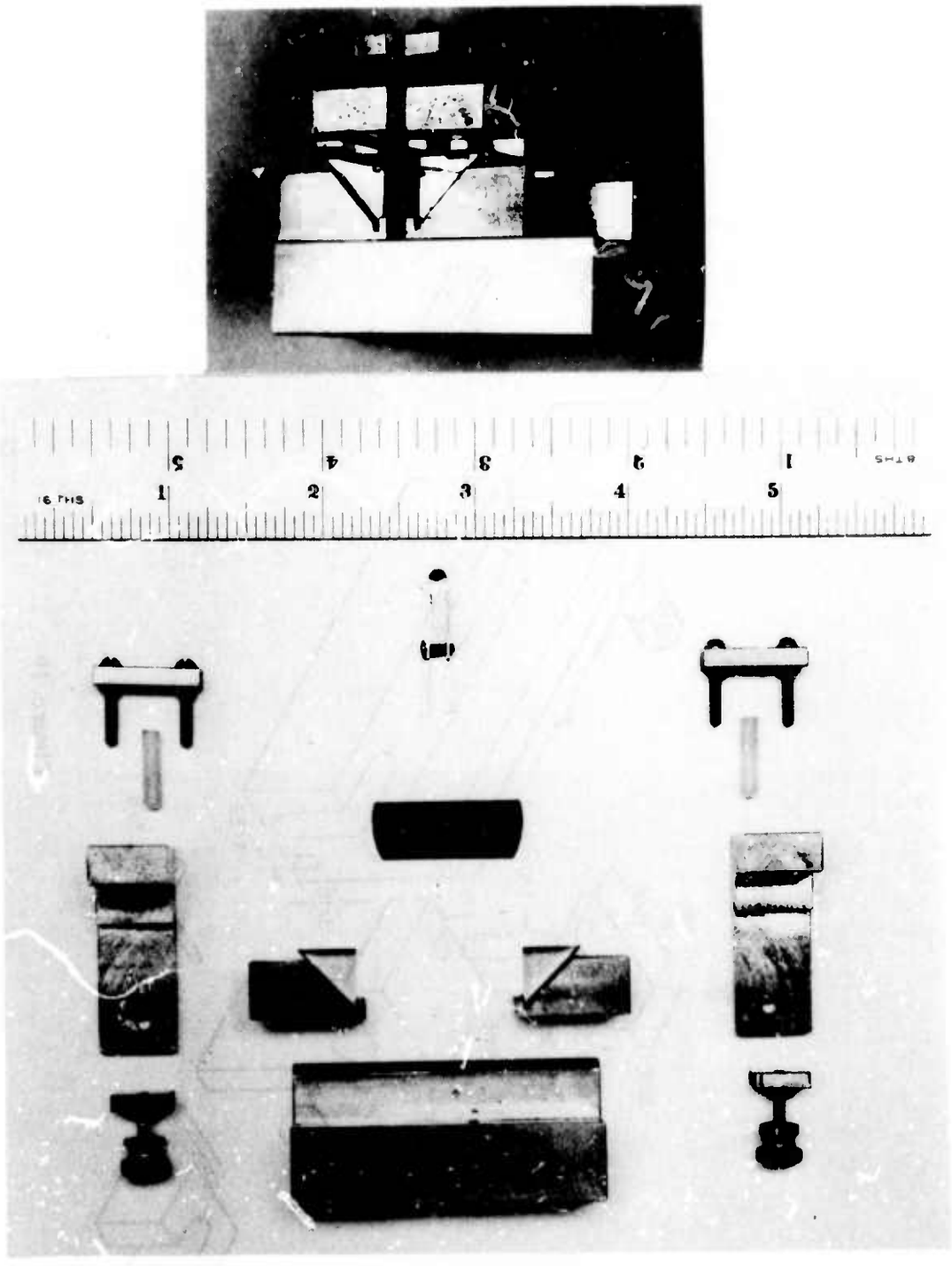

Figure 9

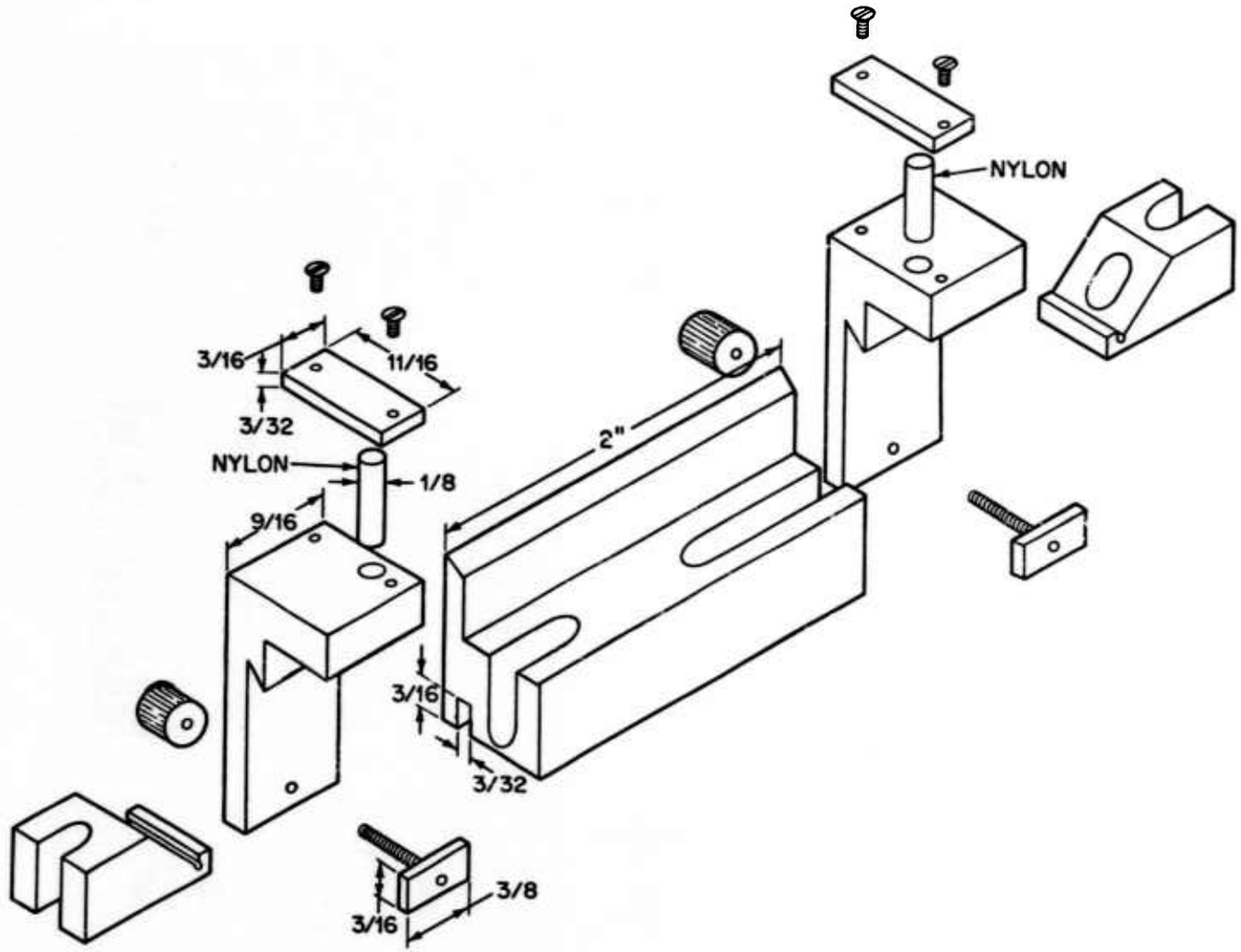

Figure 10

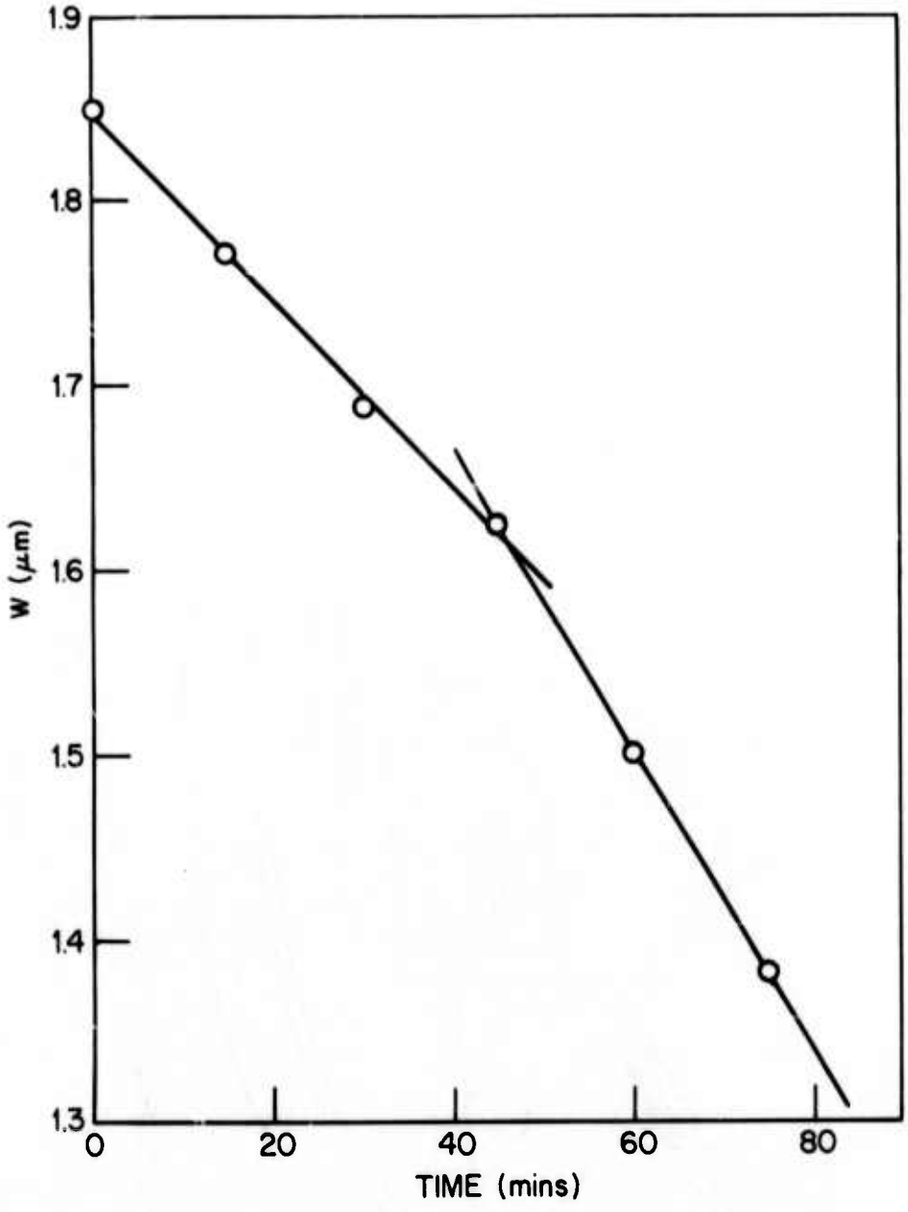

Figure 11

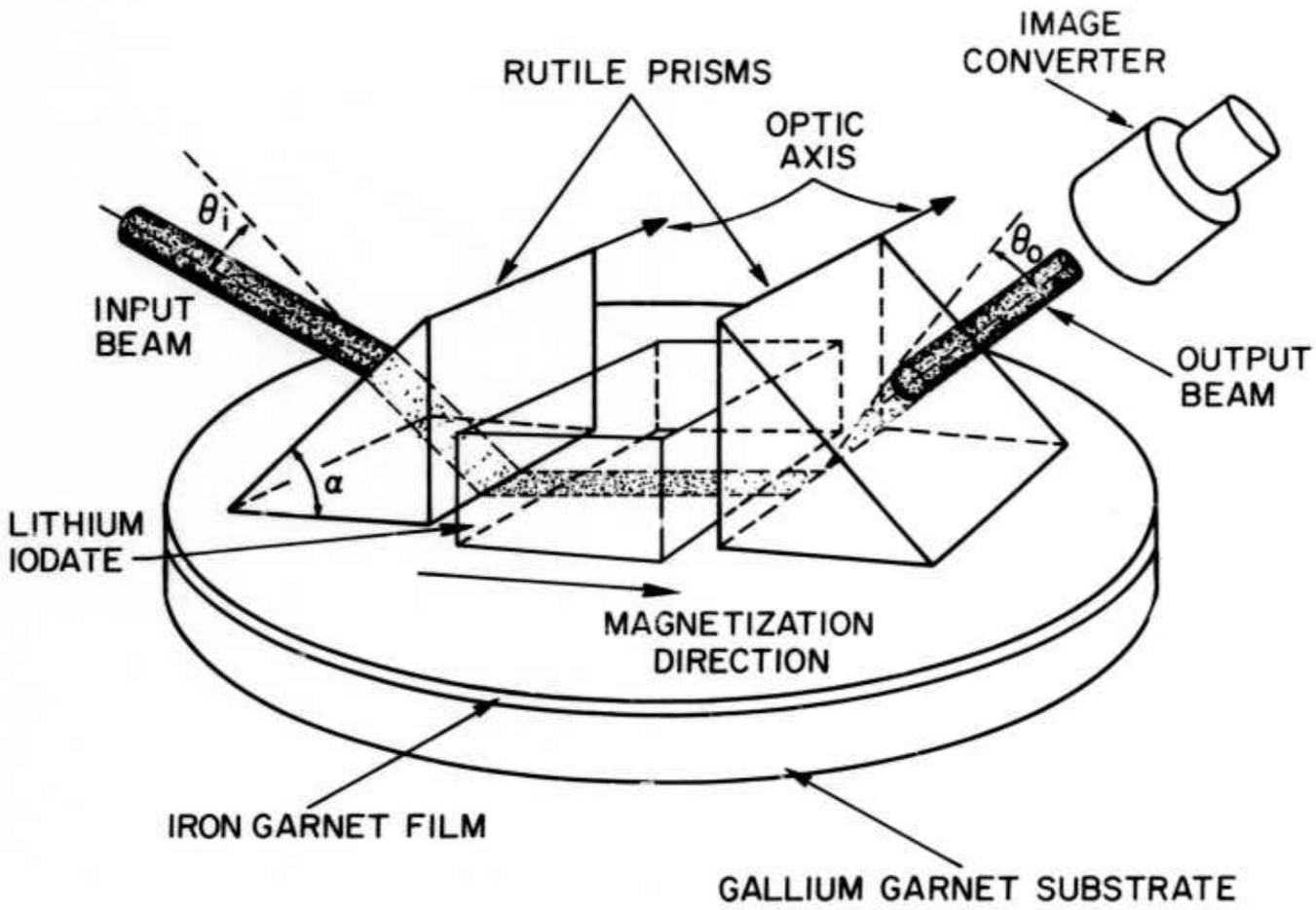
IMAGE
CONVERTER
RUTILE PRISMS
OPTIC
AXIS
θ_i
θ_o
INPUT
BEAM
OUTPUT
BEAM
α
LITHIUM
IODATE
MAGNETIZATION
DIRECTION
IRON GARNET FILM
GALLIUM GARNET SUBSTRATE

Figure 12

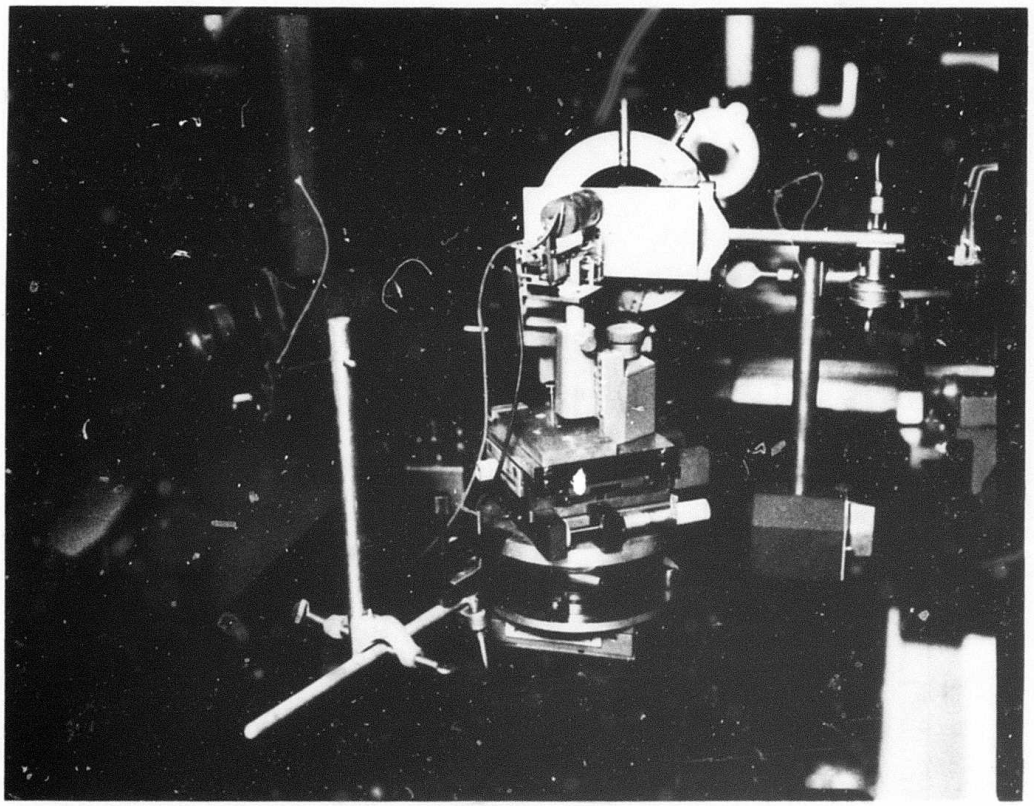

Figure 13

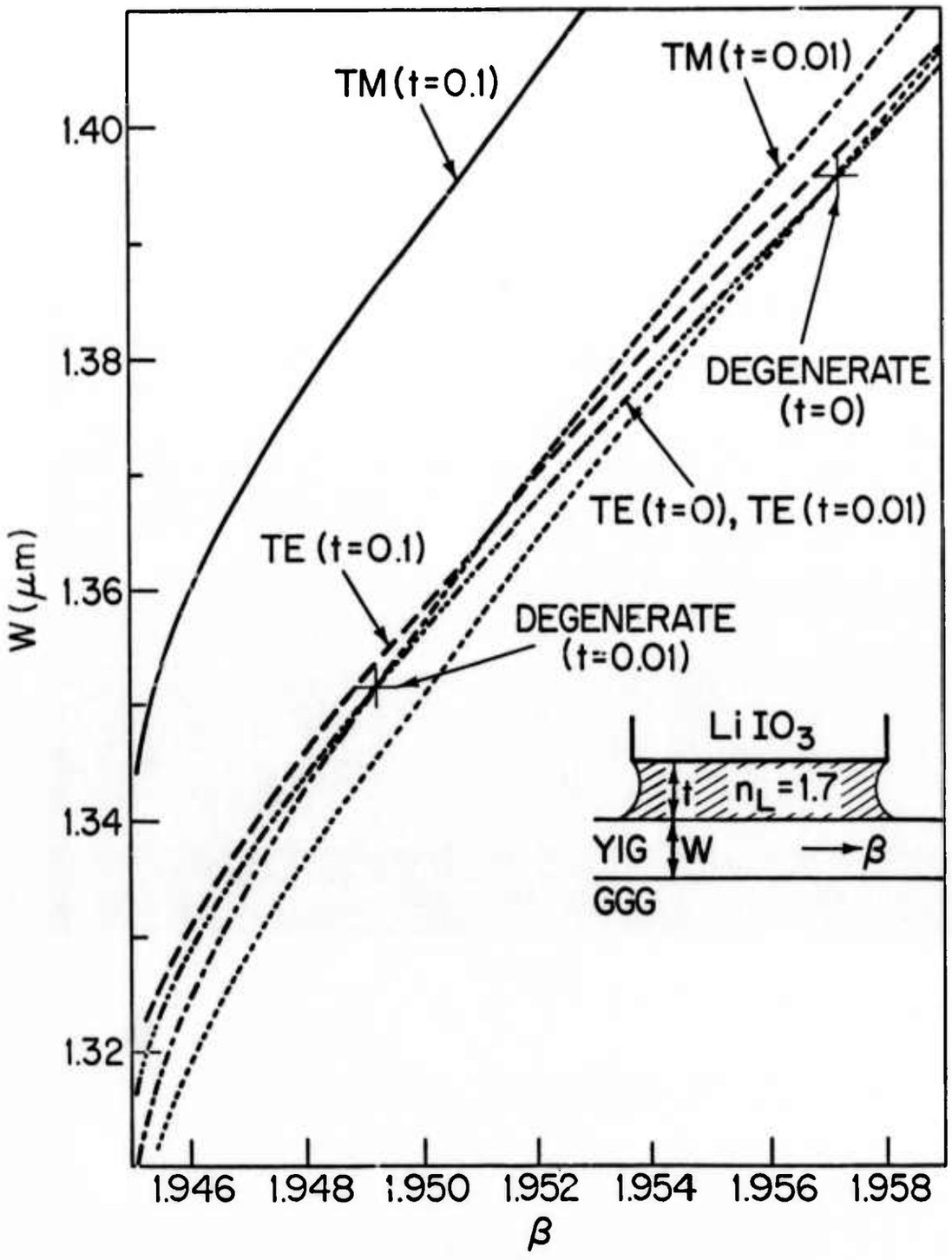
TM (t=0.1)
TM (t=0.01)
DEGENERATE
(t=0)
TE (t=0), TE (t=0.01)
TE (t=0.1)
DEGENERATE
(t=0.01)
Li IO3
t
nL=1.7
YIG
W
β
GGG
W (μm)
1.40
1.38
1.36
1.34
1.32
1.946
1.948
1.950
1.952
1.954
1.956
1.958
β

Figure 14

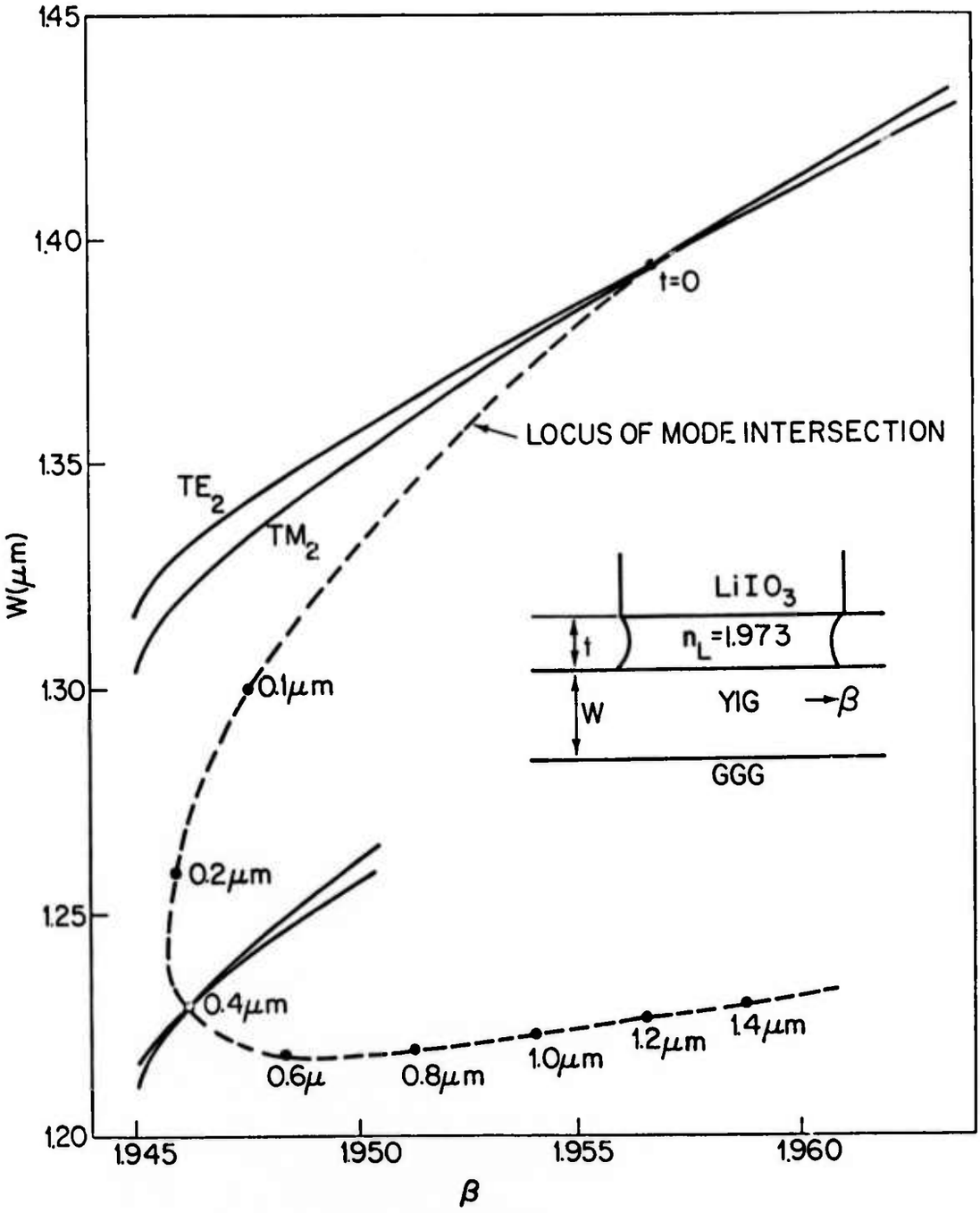
1.45
1.40
1.35
1.30
1.25
1.20
W(μm)
1.945
1.950
1.955
1.960
β
t=0
LOCUS OF MODE INTERSECTION
TE2
TM2
0.1μm
0.2μm
0.4μm
0.6μ
0.8μm
1.0μm
1.2μm
1.4μm
LiIO3
nL=1.973
t
W
YIG
β
GGG

Figure 15